

Supporting Information

For

Simultaneous Tailoring of Phase Evolution and Dopant Distribution in the Glassy Phase for Controllable Luminescence

Shifeng Zhou,^{*,†} Nan Jiang,[‡] Kiyotaka Miura,^{*,†} Setsuhisa Tanabe,[§] Masahiro Shimizu,[†] Masaaki Sakakura,[†] Yasuhiko Shimotsuma,[†] Masayuki Nishi,[†] Jianrong Qiu,^{||} and Kazuyuki Hirao[†]

[†]*Department of Material Chemistry, Graduate School of Engineering, Kyoto University, Nishikyo-ku, Kyoto 615-8510, Japan*

[‡]*Department of Physics, Arizona State University, Tempe, Arizona 85287-1504, United States*

[§]*Graduate School of Human and Environmental Studies, Kyoto University, Yoshida-Nihonmatsu-Cho Sakyo-ku, Kyoto 606-8501, Japan*

^{||}*Department of Materials Science and Engineering, Zhejiang University, Hangzhou 310027, China*

* Corresponding authors: E-mail: zhoushifeng@curl1.kuic.kyoto-u.ac.jp (S. Zhou), kmiura@collon1.kuic.kyoto-u.ac.jp (K. Miura)

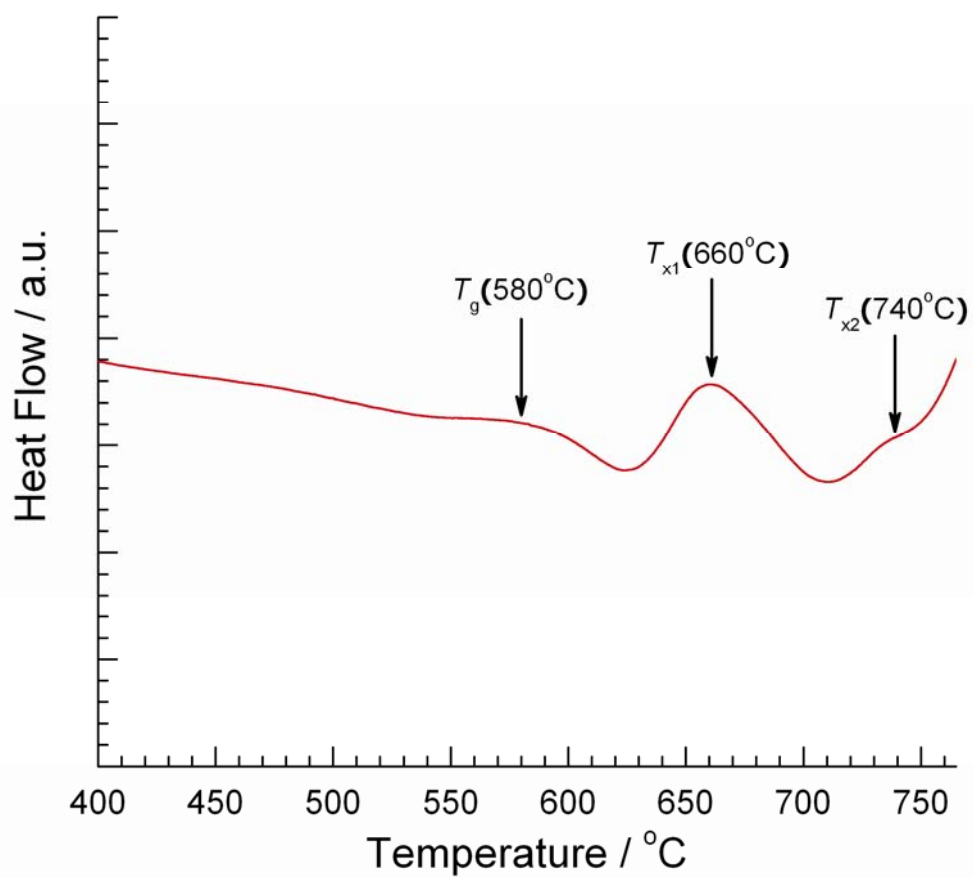


Figure S1. Differential thermal analysis of the as-made glassy phase, where T_g , T_{x1} and T_{x2} represent the glass-transition, the first and the second crystallization temperatures, respectively.

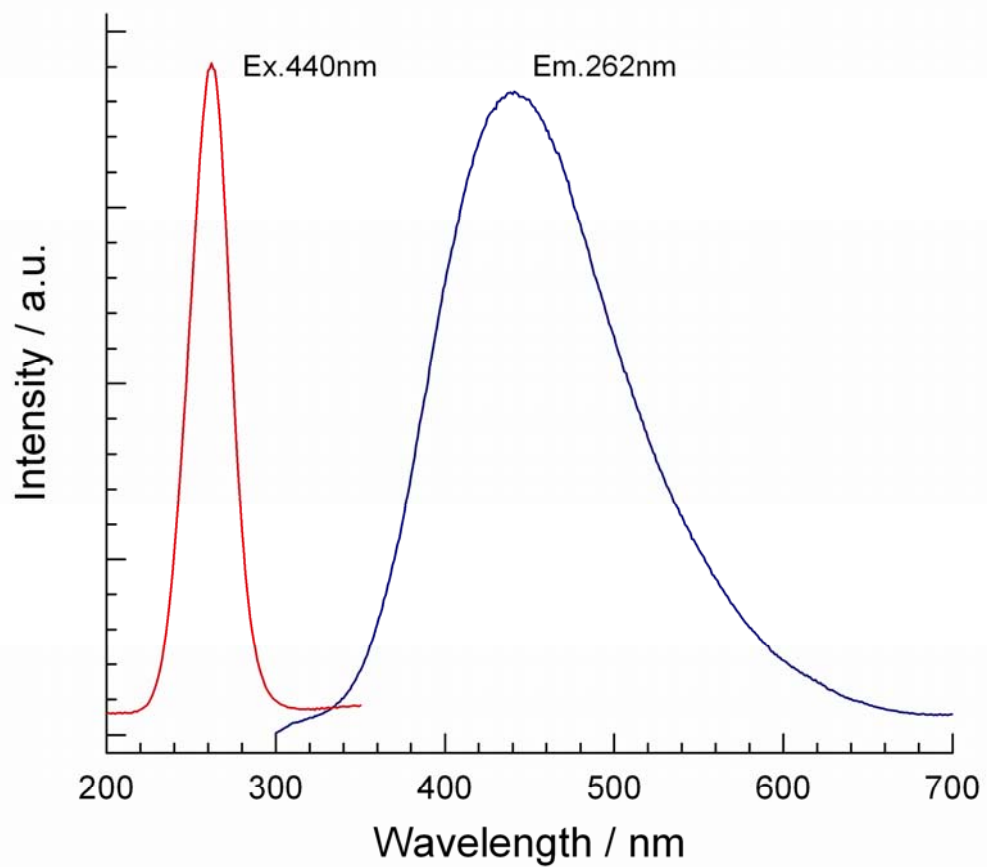


Figure S2. Photoluminescence excitation (PLE) and photoluminescence (PL) spectra of the non-doped composite heat-treated at 700 °C.

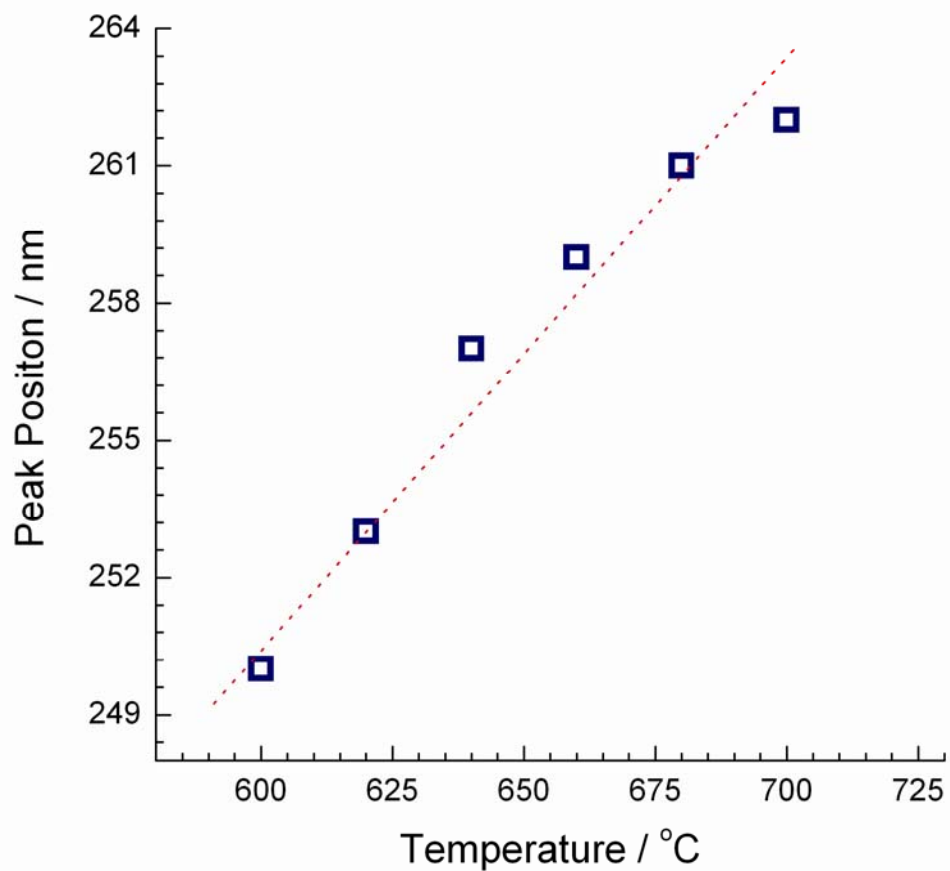


Figure S3. Heat-treatment temperature-dependent peak position of PLE spectra of the non-doped composite. The PLE spectra were measured by monitoring the luminescence at the wavelength corresponding to the peak positions shown in Fig. 2(a).

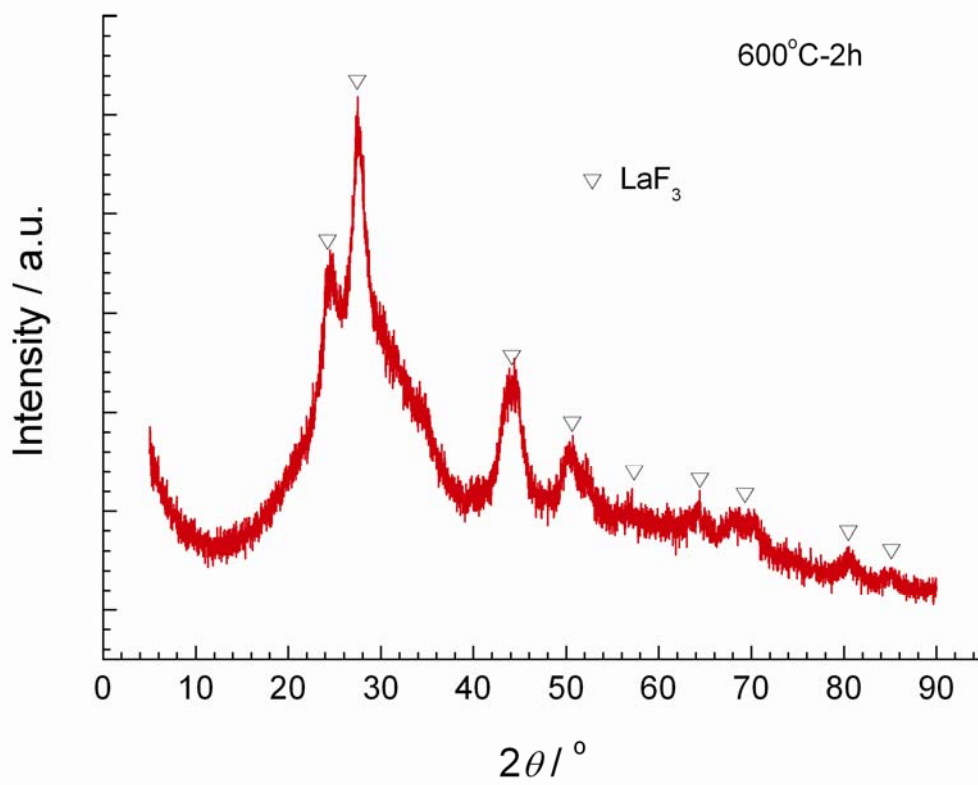


Figure S4. XRD pattern of the composite heat-treated at 600 °C for 2 h.

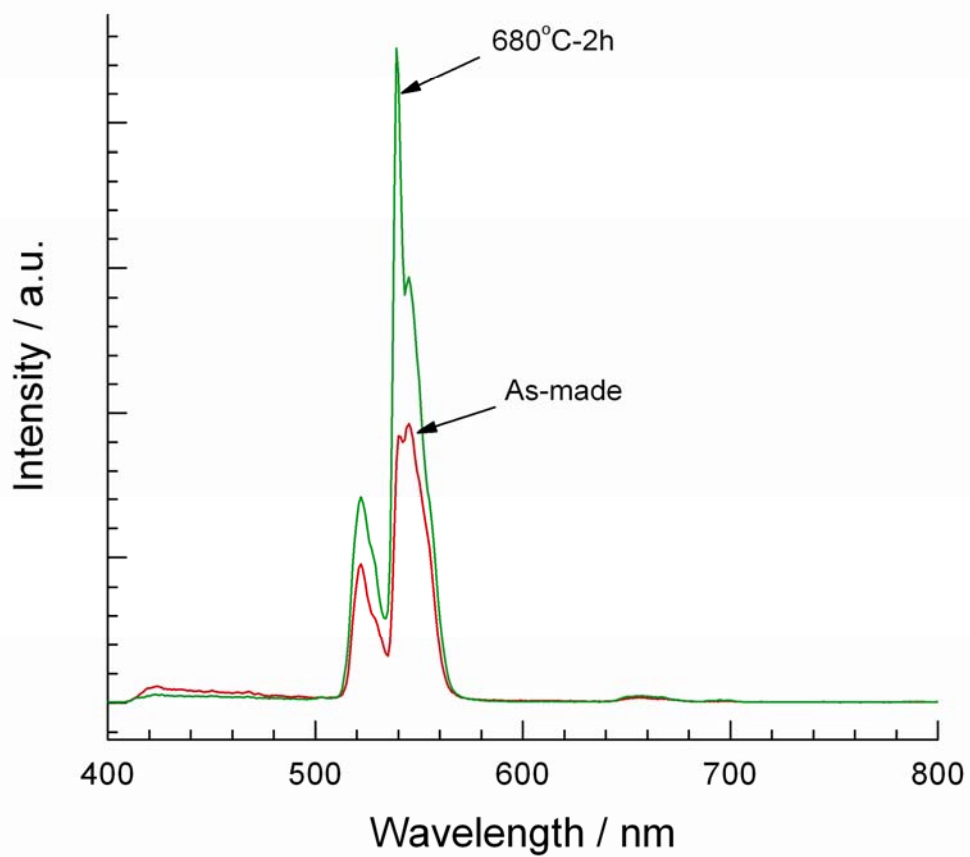


Figure S5. Luminescence spectra of Er³⁺-doped as-made glass (red line) and the composite heat-treated at 680 °C for 2 h (green line).

Table S1. Reduced matrix elements of Er^{3+} .

	$(S'L')J'$	$(SL)J$	$[U^{(2)}]^2$	$[U^{(2)}]^4$	$[U^{(2)}]^6$	$\lambda(\text{nm})$
Er^{3+}	$^4S_{3/2}$	$^4I_{15/2}$	0.0	0.0	0.2232	540
	$^2H_{11/2}$	$^4I_{15/2}$	0.7236	0.4222	0.0927	520

The Change of ligand field around rare-earth ions can be discussed by using Judd-Ofelt theory.^{2,3} According to this theory, the transition probabilities are determined by the reduced matrix elements of unit tensor operators $\langle U^{(t)} \rangle^2$ and intensity parameter Ω_t , given by equation (1).

$$A_{jj'} = \frac{64\pi^4 e^2}{3h(2J'+1)\lambda^3} \frac{n(n^2+2)^2}{9} \times \sum_{t=2,4,6} \Omega_t \left| \langle (SL)J \| U^{(t)} \| (S'L')J' \rangle \right|^2 \quad (1)$$

The calculated matrix elements of Er^{3+} ,¹ as presented in Table S1, show that the 520 and 540 nm transitions are dominated by Ω_2 and Ω_6 , respectively. These two parameters indicate the symmetry and covalency properties between Er^{3+} ions and the hosts, respectively. Ω_2 decreases with the increase of symmetry and Ω_6 increases with the decrease of covalency. It can be concluded that the change of ligand field around Er^{3+} contributes to the variation of fluorescence intensity. For example, the selective incorporation of Er^{3+} into LaF_3 nanocrystal in glass may leads to an intensity enhancement of 540 nm peak because of the decrease of covalency.

Table S2 The experimentally observed and calculated crystal field parameter (D_q), Racah parameters (B and C) and energy levels of Ni^{2+} in composite treated at 710 °C.

	Experimental (cm^{-1})	Theoretical (cm^{-1})
D_q	976	-
B	894	-
C	2982	-
${}^3\text{A}_2(\text{F}) \rightarrow {}^3\text{T}_2(\text{F})$	9728	9728
$\rightarrow {}^1\text{E}(\text{D})$	12658	13824
$\rightarrow {}^3\text{T}_1(\text{F})$	15924	15917
$\rightarrow {}^1\text{T}_2(\text{D})$	22075	23236
$\rightarrow {}^3\text{T}_1(\text{P})$	26738	26802

To calculate the crystal field and Racah parameters of Ni^{2+} , the Tanabe-Sugano matrix was solved to obtain the following expressions:⁴⁻⁶

$$D_q = \frac{\nu_1}{10} \quad (1)$$

$$B = \frac{(\nu_3 - 2\nu_1)(\nu_3 - \nu_1)}{3(5\nu_3 - 9\nu_1)} \quad (2)$$

$$C = \frac{\nu_4}{2} - 5D_q - \frac{17}{4}B + \frac{1}{4}(400D_q^2 + 40D_qB + 49B^2)^{1/2} \quad (3)$$

where ν_1 , ν_3 and ν_4 represent the electron transitions from ${}^3\text{A}_{2g}(\text{F})$ ground state to ${}^3\text{T}_{2g}(\text{F})$, ${}^3\text{T}_{1g}(\text{F})$ and ${}^3\text{T}_{1g}(\text{P})$ excited states, respectively. The D_q , B and C parameters can be calculated by applying the experimentally observed electron transitions of Ni^{2+} to the obtained expressions. The results are shown in Table S2.

By using the calculated crystal field and Racah parameters and the standard Tanabe-Sugano diagram of octahedral Ni^{2+} , the theoretical energy levels can be determined. As shown in Table S2, the fitted

energy levels are consistent with the observed absorption peaks. The location of the energy levels of Ni^{2+} in the composite treated at $710\text{ }^\circ\text{C}$ is indicated in the standard Tanabe-Sugano diagram (Fig. S6).

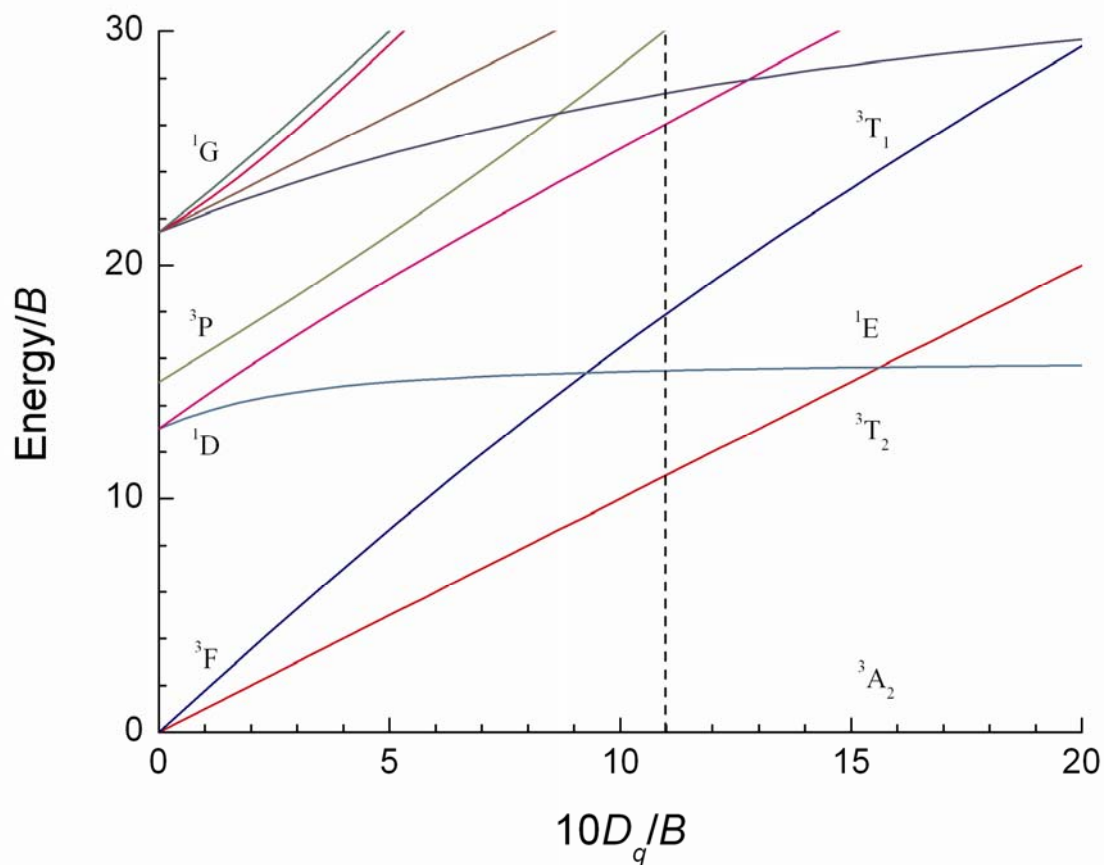


Figure S6. Tanabe-Sugano diagram of octahedral Ni^{2+} . Vertical dashed line shows the location of the energy levels of Ni^{2+} in the composite treated at $710\text{ }^\circ\text{C}$.

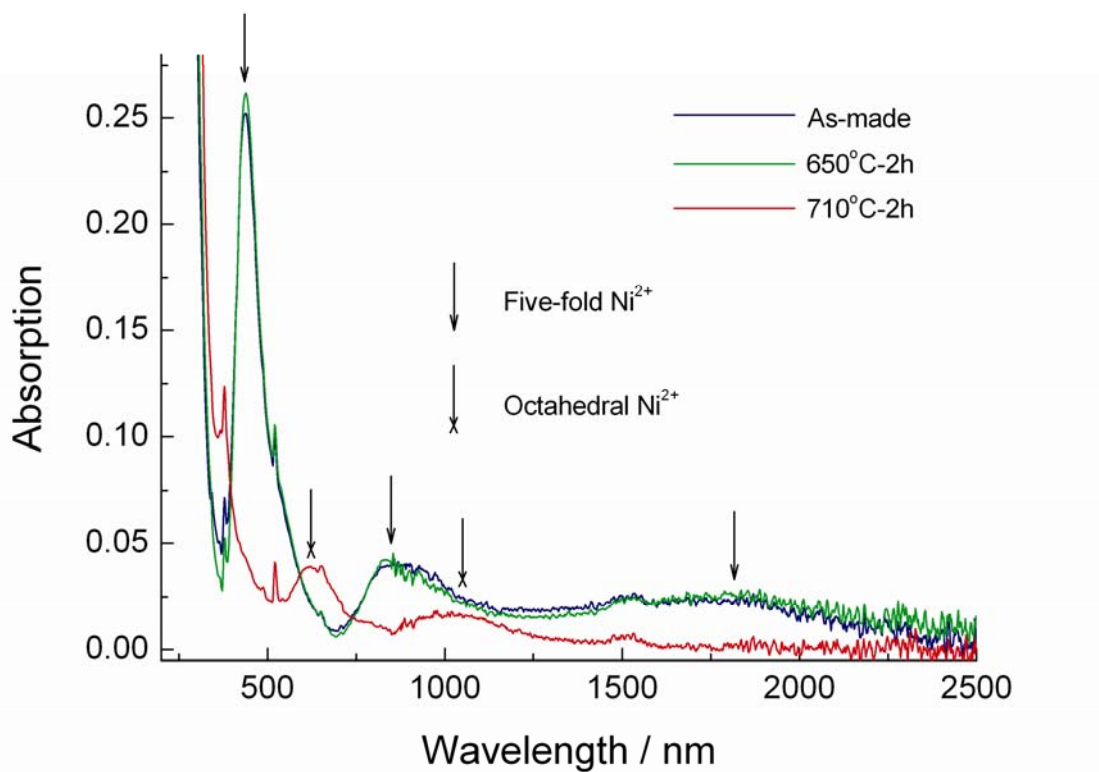


Figure S7. Absorption spectra of Ni²⁺-Er³⁺ codoped glass and the composite heat-treated at 650 and 710 °C, respectively. The arrows indicate the origin of absorption bands. The results show that the characteristic absorption bands of five-fold Ni²⁺ absolutely disappear during the precipitation of Ga₂O₃ nanocrystals, demonstrating the selective partition of Ni²⁺ into Ga₂O₃.

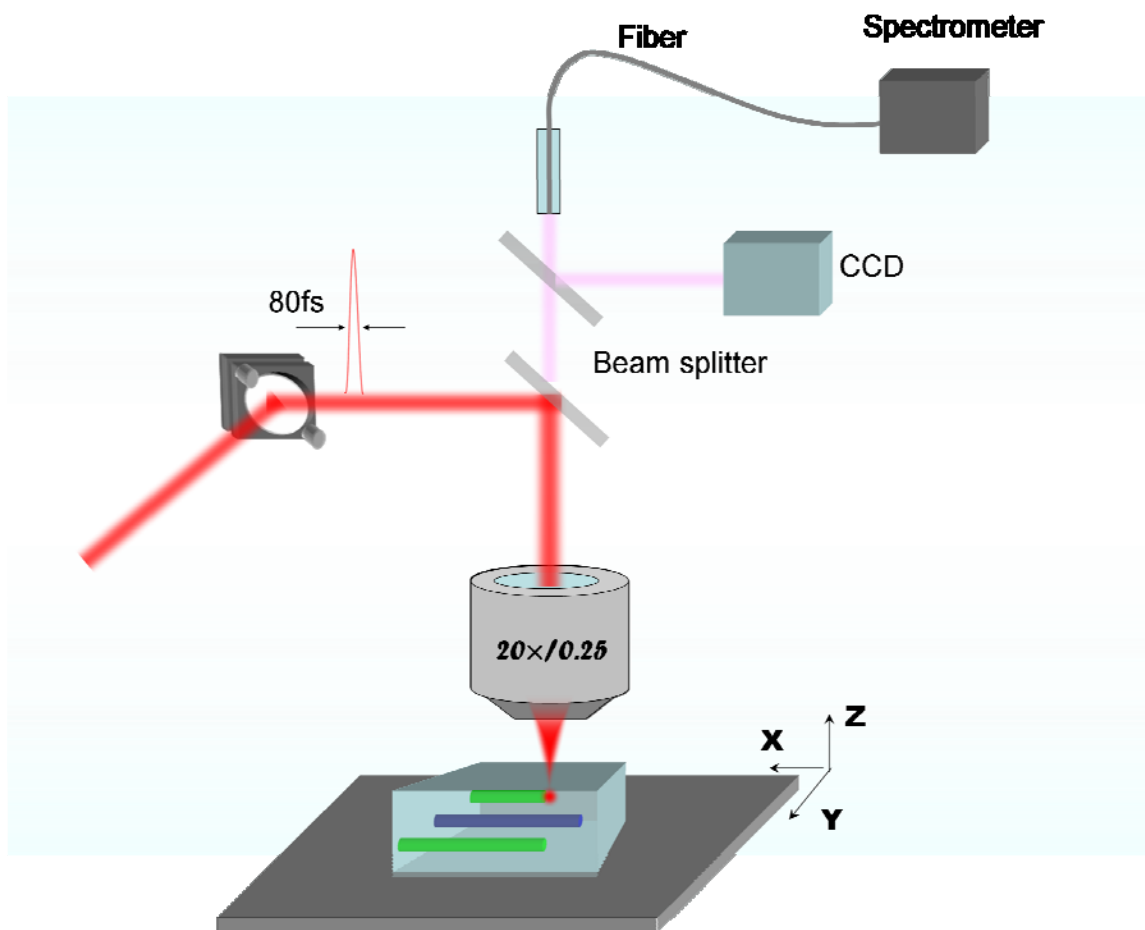


Figure S8. Schematic illustration of the experimental setup for space-selective micro-fabrication and upconversion luminescence measurement.

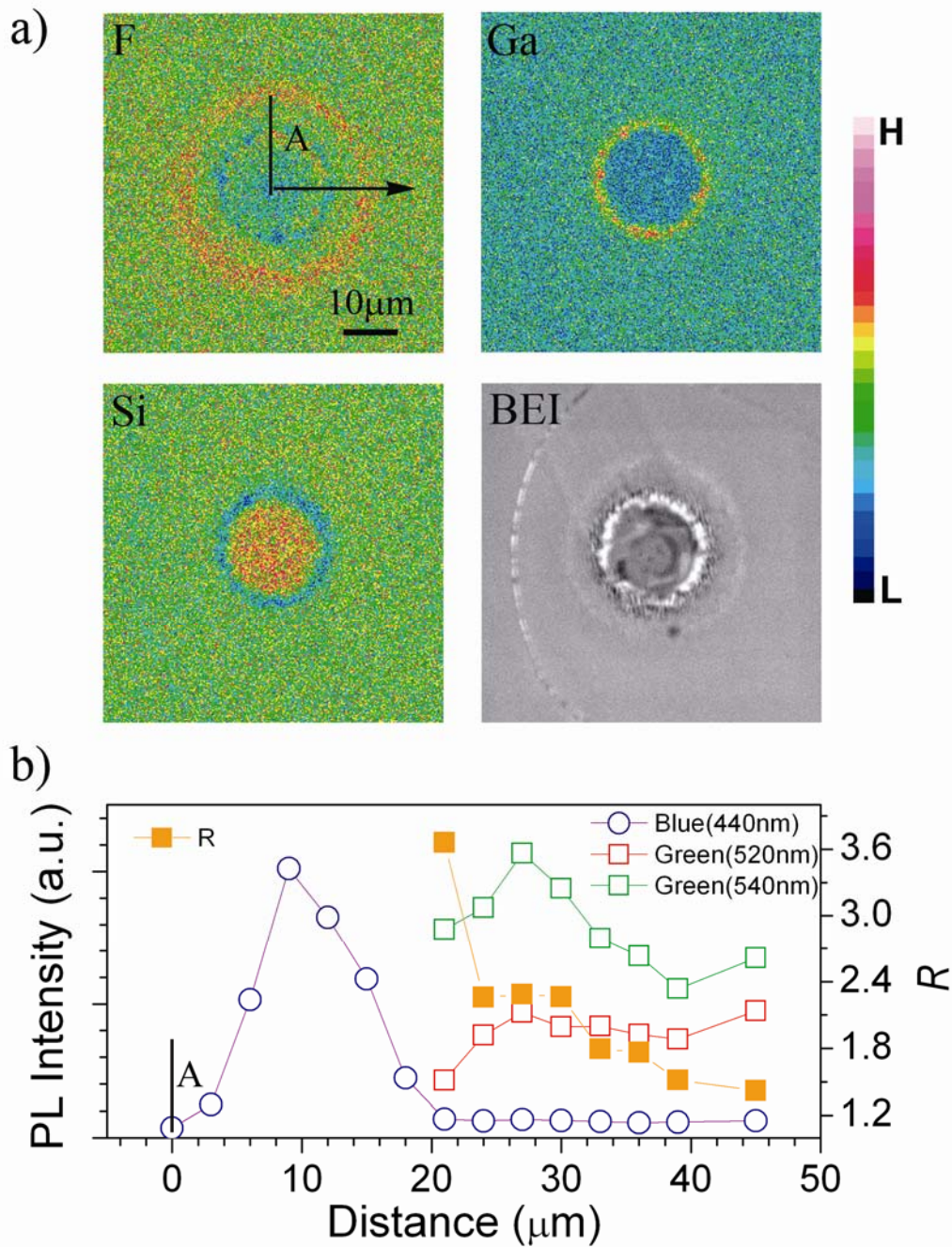


Figure S9. a) Ions distribution (F, Ga and Si) map and backscattering electron image (BEI) around the ultra-short pulse laser modified region, measured by EPMA. b) Photoluminescence investigation of the modified region via scanning the excitation laser from point A and along the direction marked by black arrow shown in a).

References:

- (1) Tanabe S.; Hayashi H., Hanada T.; Onodera N. *Opt. Mater.* **2002**, *19*, 343-349.
- (2) Judd B. R. *Phys. Rev.* **1962**, *127*, 750-761.
- (3) Tanabe S.; Ohyagi T.; Soga N.; Hanada T. *Phys. Rev. B* **1992**, *46*, 3305-3310.
- (4) Tanabe Y.; Sugano S. *J. Phys. Soc. Jpn.* **1954**, *9*, 753-766.
- (5) Tanabe Y.; Sugano S. *J. Phys. Soc. Jpn.* **1954**, *9*, 766-779.
- (6) Shigemura H.; Shojiya M.; Kanno R.; Kawamoto Y. *J. Phys. Chem. B* **1998**, *102*, 1920-1925.